

# Impact ionisation in $\text{Al}_{0.9}\text{Ga}_{0.1}\text{As}_{0.08}\text{Sb}_{0.92}$ for Sb-based avalanche photodiodes

*X. Collins, A. P. Craig, T. Roblin, and A. R. J Marshall*

*Physics Department, Lancaster University, Lancaster, LA1 4YB, UK*

## Abstract

We report the impact ionisation coefficients of the quaternary alloy  $\text{Al}_{0.9}\text{Ga}_{0.1}\text{As}_{0.08}\text{Sb}_{0.92}$  lattice matched to GaSb substrates within the field range of 150 to 550  $\text{kVcm}^{-1}$  using *p-i-n* and *n-i-p* diodes of various intrinsic thicknesses. The coefficients were found with an evolutionary fitting algorithm using a non-local recurrence based multiplication model and a variable electric field profile. These coefficients not only indicate that an avalanche photodiode can be designed to be function in the mid-wave infrared, but also can be operated at lower voltages. This is due to the high magnitude of the impact ionisation coefficients at relatively low fields compared to other III-V materials typically used in avalanche multiplication regions.

Avalanche photodiodes (APDs) can offer high signal to noise ratios through internal gain due to impact ionisation. Within the infrared (IR), Si based APDs have been predominant for wavelengths up to 1.1  $\mu\text{m}$ <sup>1</sup> while for the most commonly used telecoms wavelengths of 1.3 and 1.55  $\mu\text{m}$ , InGaAs/AlInAs based separate absorption and multiplication (SAM) APDs have become the incumbent technology after much study<sup>2</sup>. However few examples of APDs operating at extended IR wavelengths exist<sup>3-5</sup> especially with III-V materials. These APDs would be useful in applications such as imaging, ranging and communicating through obscurant media<sup>6</sup>, where photon fluxes are low and the use of longer wavelengths can be desirable. InAs is a material which due to its low band gap it can absorb beyond telecoms wavelengths of 1.3 and 1.55  $\mu\text{m}$ , and also benefits from highly dissimilar ionisation coefficients resulting in low noise multiplication<sup>4</sup>. However unfortunately it is highly susceptible to tunnelling currents as a result of its low band gap and electron effective mass, therefore compromised for APD applications. Hence, it would be highly desirable to develop SAM APDs based on Sb-materials lattice matched to a GaSb substrate. This has been achieved recently with AlInAsSb based SAM APDs<sup>7</sup>. However, they have only been demonstrated up to a cut-off wavelength of 1.6  $\mu\text{m}$ , and impact ionisation coefficients for AlInAsSb, which are crucial in designing a SAM APD, have not been published.

We present a study of the impact ionisation in  $\text{Al}_{0.9}\text{Ga}_{0.1}\text{As}_{0.08}\text{Sb}_{0.92}$ , hereafter referred to as AlGaAsSb. Being lattice matched to GaSb, this would support SAM APDs with Sb-based absorbers such as InGaAsSb, InAsSb or even strained layer superlattices (SLs), covering the short, mid and longwave regions respectively. In order to design SAM APDs, the impact ionisation coefficients reported here are required to determine the electric field necessary for adequate multiplication and the charge sheet thickness required for low field in the low band gap absorber.

Phase sensitive measurements of pure electron and hole photomultiplication were made using a series of *p-i-n* and *n-i-p* diodes of several thicknesses. Non-local ionisation coefficients were then established using a variable field recurrence based multiplication model<sup>8</sup> via an evolutionary fitting algorithm. The coefficients are parameterised and compared to those for other III-V materials.

All samples were grown using a Veeco GENxplor MBE reactor equipped with valved cracker cells for As and Sb and SUMO cells for Al, Ga and In. Epi-ready GaSb *n*-type and *p*-type substrates were used for *p-i-n* and *n-i-p* diodes respectively. Oxide desorption was carried out at 530 °C. The substrate was then cooled to 500 °C for growth, which was carried out with a V/III growth rate ratio of 2.2 and an overall group III rate of 1 MLs<sup>-1</sup>. After a GaSb buffer, the AlGaAsSb diode structures were grown using Te and Be for the *n* and *p*-type dopants respectively. Doping concentrations were approximately determined from Hall effect measurements on calibration growths, these values were subsequently refined by fitting to the CV measurements. The *p*-side doping concentration in all devices was  $1 \times 10^{18}$  cm<sup>-3</sup>, and the *n* doping concentration was  $3 \times 10^{17}$  cm<sup>-3</sup>. The upper AlGaAsSb claddings were grown to be many times thicker than required for extinction of the laser used, ensuring pure carrier injection. A thin contact layer was grown for each wafer with GaSb used on the *p-i-n* devices and, to ensure an Ohmic contact, InAs used on the *n-i-p* device. These contact layers additionally served to prevent oxidation of the wafer surfaces. Figure 1 shows the structure of the thin *p-i-n* diode. In addition to this device, a *p-i-n* diode with a thicker intrinsic region of 300 nm was grown as well as a complementary *n-i-p* diode with the same intrinsic thickness as the thin *p-i-n*. Processing was carried out using standard photolithography, Ti/Au contact metallisation and a low concentration HF based wet etchant. Mesa diodes with diameters between 100 to 800 μm were fabricated for characterisation.

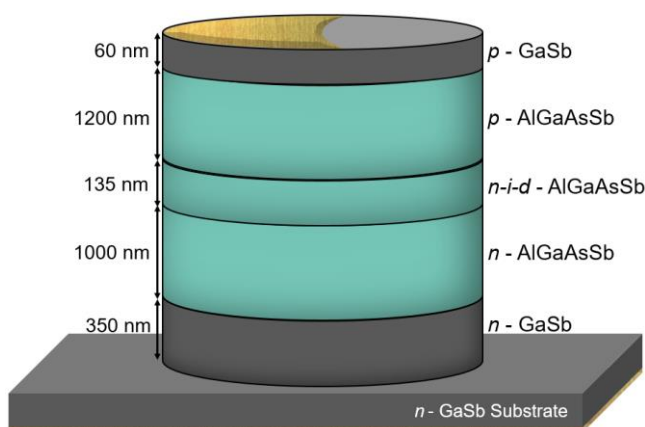


Figure 1: Layer structure for the thin  $p-i-n$  diode. Additionally, a complementary  $n-i-p$  structure with 135 nm intrinsic width was grown, along with a thicker  $p-i-n$  diode with a 300 nm intrinsic width.

Multiplication measurements were carried out by phase sensitive detection ensuring the effect measured was photomultiplication rather than any effect associated with dark current. The chopped laser was fibre coupled to the centre of the device using a multimode fibre with a core diameter of 50  $\mu\text{m}$ , thus illuminating an area smaller than the device diameter to ensure pure electron or hole injection. An SRS SR830 lock-in amplifier and Keithly 2400 Sourcemeter® were used for phase sensitive detection and biasing respectively. CV measurements were carried out using an Agilent E4980 LCR meter. The device structures described above were verified using CV measurements fitted using a Poisson equation model. The thicknesses of the intrinsic widths are the results of the CV simulations including a step grading doping profile to account for any dopant diffusion. The thickness are given to the nearest 5 nm to account for uncertainty in the boundary of the intrinsic and the doped layer. The area dependence of the capacitance density was verified using the measured device diameters. It was found that the capacitance density varied by a maximum of  $\pm 1\%$  across diameters of 100 to 800  $\mu\text{m}$ . Fitted CV curves, along with experimental data, are shown in figure 2 for all three devices.

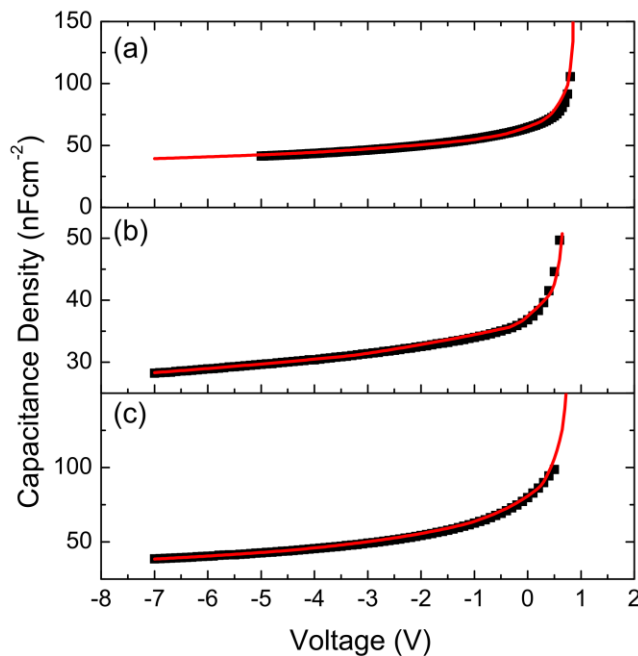


Figure 2: Capacitance voltage measurements for the (a) 135 nm intrinsic width  $p-i-n$ , (b) 300 nm intrinsic width  $p-i-n$  and (c) 135 nm intrinsic width  $n-i-p$ . Solid line represent simulated data while the symbols show experimentally found data, confirmed to be consistent across device diameters.

The primary photocurrent generated in  $p-i-n$  and  $n-i-p$  photodiodes is known to vary with the depletion width, hence this was fitted at low bias allowing the multiplication factor to be calculated accurately<sup>9</sup>. The multiplication resulting from both pure electron and pure hole injection is shown on figure 3. These results were measured on devices with a range of diameters, to ensure area independence. Additionally the multiplication was modelled for comparison and use in fitting the ionisation coefficients. This was achieved using the method of recurrent integrals with a hard threshold dead space, as described by Hayat *et al.*<sup>8</sup>.

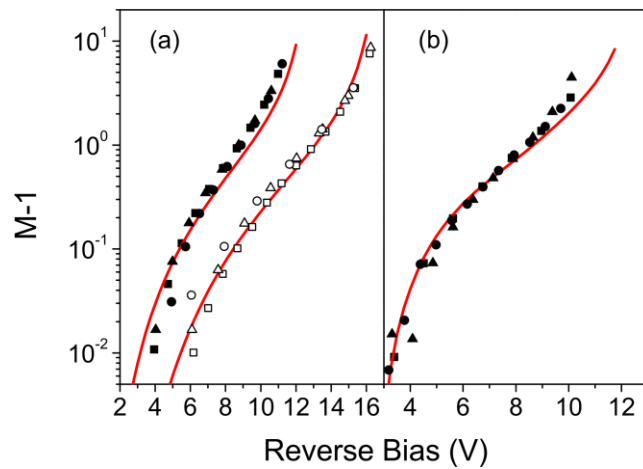


Figure 3: Multiplication for (a)  $p-i-n$  structures and (b)  $n-i-p$  structure as a function of reverse bias for 135 nm (■) and 300 nm (□) intrinsic widths. Square (■) and circle (●) symbols indicate devices with a diameter of 400  $\mu\text{m}$  while triangle (▲) symbols represent 200  $\mu\text{m}$  diameter devices. The lines show simulated  $M_e$  (a) and  $M_h$  (b), calculated using the fitted ionisation coefficients and the diodes respective electric field profiles.

By chi-squared reduction, an evolutionary algorithm was used to fit the electric field dependent impact ionisation coefficients for electrons ( $\alpha$ ) and holes ( $\beta$ ) in the parameterised form given by equation 1, where  $A$ ,  $B$  and  $C$  are fitting parameters and  $E$  is electric field<sup>10</sup>. The values for electron and hole threshold energies,  $E_{\text{th}(e)}$  and  $E_{\text{th}(h)}$  respectively, were also simultaneously found from the fitting.

$$\alpha = A \exp \left[ - \left( \frac{B}{E} \right)^C \right] \quad (1)$$

The evolutionary algorithm converged to the non-local impact ionisation coefficients in equations 2 and 3. These are valid for an electric field range of 150 - 550 kVcm<sup>-1</sup> with ionisation threshold energies of  $E_{th(e)} = 1.74$  eV and  $E_{th(h)} = 3.38$  eV. The coefficients are plotted in figure 4, which also compares them to the reported coefficients for selected III-V materials.

$$\alpha = 1.22 \times 10^7 \exp\left(-\left(\frac{6.21 \times 10^6}{E}\right)^{0.671}\right) \text{ cm}^{-1} \quad (2)$$

$$\beta = 1.22 \times 10^7 \exp\left(-\left(\frac{1.11 \times 10^7}{E}\right)^{0.536}\right) \text{ cm}^{-1} \quad (3)$$

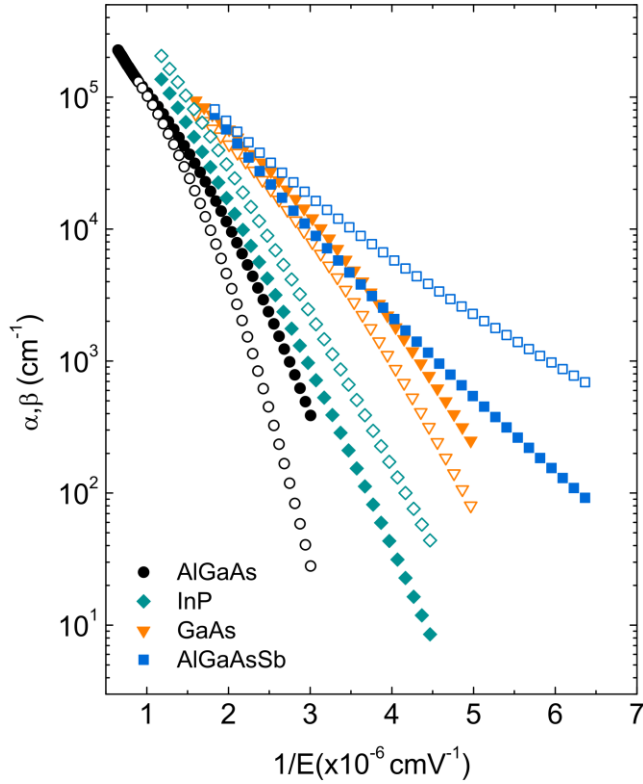


Figure 4: A comparison of the obtained coefficients for AlGaAsSb with those reported for Al<sub>0.8</sub>Ga<sub>0.2</sub>As<sup>11</sup>, GaAs<sup>12</sup> and InP<sup>13</sup>. Solid symbols represent the electron ionisation coefficients and open symbols represent the hole ionisation coefficients.

The breakdown voltage of the thinnest devices sets the upper limit of the field range of our impact ionisation coefficients. As can be seen from figure 4, the impact ionisation coefficients for AlGaAsSb are higher over the investigated field range than other III-V materials. Furthermore, the hole coefficient is higher than the electron coefficient which is uncommon among the III-V materials, but does feature in InP, certain compositions of AlGaSb<sup>14</sup> and lower Al concentrations of AlGaAsSb<sup>15</sup>. Grzesik et al.<sup>15</sup> reported that  $\beta > \alpha$  in  $\text{Al}_x\text{Ga}_{1-x}\text{As}_y\text{Sb}_{1-y}$  for  $x = 0.55$  and  $y = 0.045$  over the investigated field range of  $160 - 400 \text{ kVcm}^{-1}$ . As an alternative material lattice matched to GaSb, the alloy AlInAsSb has been found to exhibit  $\alpha > \beta$ <sup>7</sup>, however the alloy compositions studied differ significantly from the AlGaAsSb reported in this work.

Due to the majority of the III-V materials behaving differently, this property has been investigated previously. For InP Brennan *et al.*<sup>16</sup> proposed that the reversal in the coefficient ratio, such that  $\beta > \alpha$ , is caused by the difference between in the ionisation threshold energies,  $E_{\text{th}(e)} = 2.10 \text{ eV}$  and  $E_{\text{th}(h)} = 1.55 \text{ eV}$ . However, more recent studies have reported similar ionisation threshold energies for electrons and holes. Saleh *et al.*<sup>17</sup> fitted  $E_{\text{th}(e)} = 2.05 \text{ eV}$  and  $E_{\text{th}(h)} = 2.20 \text{ eV}$ , while Tan *et al.*<sup>13</sup> fitted  $E_{\text{th}(e)} = 2.8 \text{ eV}$  and  $E_{\text{th}(h)} = 3.0 \text{ eV}$ . Hence these results do not support the theory of Brennan *et al.*<sup>16</sup> and show that a higher hole ionisation coefficient and hole threshold energy are not mutually exclusive, as also observed in this work.

Hildebrand *et al.*<sup>14</sup> put a different proposal forward to explain their finding that  $\beta > \alpha$  in AlGaSb. They concluded that the hole coefficient exhibited “resonant enhancement” when the valence band spin-orbit split-off energy ( $\Delta_{SO}$ ) was equal to the direct band gap energy ( $E_g^{\Gamma}$ ). Since the composition of our material is so AlSb-rich and the bowing parameter for the split off band is unknown, we estimate  $\Delta_{SO}$  to be approximately equal to that for AlSb,  $0.676 \text{ eV}$ <sup>18</sup>. In comparison we calculate  $E_g^{\Gamma}$  to be  $2.01 \text{ eV}$ <sup>18</sup> and the ratio  $\Delta_{SO}/E_g^{\Gamma}$  as  $0.34$ , far away from the value of 1 where resonance is proposed to occur. Hence following our initial study, we can only conclude that  $\beta > \alpha$  in AlGaAsSb due to a lower average scattering rate for holes compared to electrons, at the elevated energies required for ionisation.

If the intrinsic width of a  $p-i-n$  APD is reduced tunnelling currents become increasingly significant, eventually dominating the total leakage current with deleterious effects on the signal to noise ratio. In comparison to other III-V materials, it is noteworthy that no tunnelling currents were observed in the AlGaAsSb diodes, despite the minimum investigated intrinsic region thickness of only 135 nm. The absence of tunnelling currents was confirmed by temperature dependent leakage current characterisation. In light of this, it should be possible to extend the ionisation coefficient electric field range to higher values in the future using thinner intrinsic widths. In general, the minimum useful intrinsic width for a given material principally depends upon its bandgap and the magnitude of its ionisation coefficients. In the case of AlGaAsSb it is proposed that both the high ionisation coefficients, as shown in figure 4, and a large  $E_g^I$  contribute to even the thinnest diodes reaching desirable avalanche breakdown before any tunnelling becomes evident. AlGaAsSb has a direct bandgap energy  $E_g^I = 2.01$  eV<sup>18</sup> which is significantly larger than those of GaAs (1.42 eV) and InP (1.34 eV)<sup>1</sup>, hence presenting a higher potential barrier and suppressing tunnelling probability. In this comparison, the direct bandgap energy is used, since a momentum change would be required for an electron to tunnel into the  $X$ -valley, which lies below the  $\Gamma$ -valley.

As a consequence of the high ionisation coefficients, suppressed tunnelling and usable thin intrinsic widths, we believe AlGaAsSb APDs can be designed with a lower operating voltage than has been achieved with other III-V materials. To test this the multiplication within  $p-i-n$  APDs, with the same 135 nm intrinsic thickness as our thinnest device, was modelled using the impact ionisation coefficients reported for different III-V materials<sup>11-13</sup>. As shown in figure 5, the AlGaAsSb  $p-i-n$  APD displays an increased multiplication factor at all reverse biases, compared to GaAs, InP and Al<sub>0.8</sub>Ga<sub>0.2</sub>As. By extension, a SAM APD with a multiplication region of AlGaAsSb, as proposed earlier, would also require a lower operating bias. Furthermore, for the 135 nm intrinsic width modelled, GaAs and InP would be susceptible to tunnelling currents as shown in the inset in figure 5. The tunnelling current in InP has been calculated as described by Forrest *et al.*<sup>19</sup> using the values obtained by Tan *et al.*<sup>13</sup>, while GaAs has been modelled using the work of Benz *et al.*<sup>20</sup>. From these models, we find that at an operating

multiplication factor of 11, the tunnelling currents for GaAs and InP are  $17.7 \text{ mAcm}^{-2}$  and  $3.5 \text{ mAcm}^{-2}$  respectively. This would clearly introduce undesirable noise in comparison to the AlGaAsSb APD.

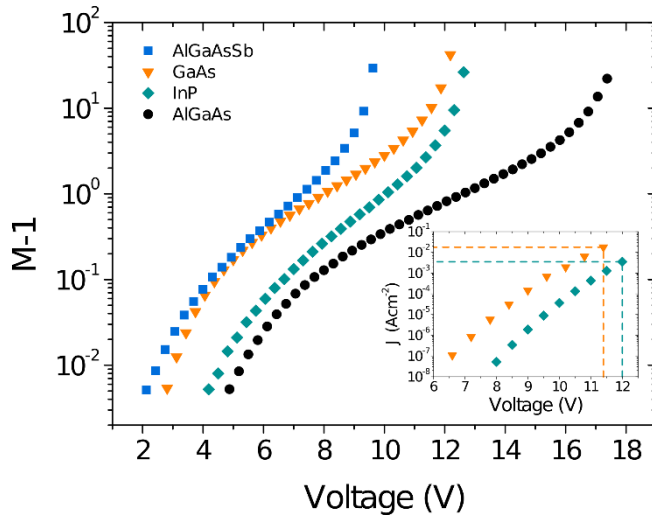


Figure 5: A comparison of simulated multiplication for *p-i-n* APDs with 135 nm intrinsic widths using different materials. Inset: the tunnelling current ( $J$ ) in the GaAs and InP *p-i-n* APDs. Dashed lines represent the tunnelling current at a typical operating voltage where  $M = 11$ .

Over a field range of  $150$  to  $550 \text{ kVcm}^{-1}$ , we report the electron and hole impact ionisation coefficients of AlGaAsSb. These were found by using an evolutionary fitting algorithm, which took into consideration the positional dependence of the electric field and calculated the multiplication for candidate coefficients. An ionisation threshold energy was implemented to account for the dead space traversed by injected and ionised carriers. The electron and hole coefficients are found to be atypically high indicating the material's suitability for use in low operating voltage GaSb-based SAM APDs, supporting applications in the extended IR.

The authors would like to thank Innovate UK for providing funding under project #102675 and the Centre for Defence Enterprise (DSTL1000108318). The authors also wish to thank the UK Engineering and Physical Sciences Research Council for the studentship provided to X. Collins (grant number EP/N50950411). United Kingdom Patent Application No. 1711138.6.

- <sup>1</sup> S.M. Sze and K.K. Ng, *Physics of Semiconductor Devices*, 3rd ed. (John Wiley & Sons, Inc., Hoboken, New Jersey, 2007).
- <sup>2</sup> M. Lahrichi, G. Glastre, E. Derouin, D. Carpentier, N. Lagay, J. Decobert, and M. Achouche, *IEEE Photonics Technol. Lett.* **22**, 1373 (2010).
- <sup>3</sup> J. Beck, C. Wan, M. Kinch, J. Robinson, P. Mitra, R. Scritchfield, F. Ma, and J. Campbell, *J. Electron. Mater.* **35**, 1166 (2006).
- <sup>4</sup> A.R.J. Marshall, J.P.R. David, and C.H. Tan, *IEEE Trans. Electron Devices* **57**, 2631 (2010).
- <sup>5</sup> A.P. Craig, C.J. Reyner, A.R.J. Marshall, and D.L. Huffaker, *Appl. Phys. Lett.* **104**, 1 (2014).
- <sup>6</sup> S.D. Lord, NASA Technical Memorandum 103957 (1992).
- <sup>7</sup> S.R. Bank, S. Member, J.C. Campbell, S.J. Maddox, M. Ren, A. Rockwell, M.E. Woodson, and S.D. March, *IEEE J. Sel. Top. Quantum Electron.* **24**, (2018).
- <sup>8</sup> M.M. Hayat, B.E. Saleh, and M.C. Teich, *IEEE Trans. Electron Devices* **39**, 546 (1992).
- <sup>9</sup> M.H. Woods, W.C. Johnson, and M.A. Lampert, *Solid. State. Electron.* **16**, 381 (1973).
- <sup>10</sup> G.E. Stillman and C.M. Wolfe, in *Semicond. Semimetals*, 12th ed. (Academic Press, inc, London, 1977).
- <sup>11</sup> B.K. Ng, J.P.R. David, S. a. Plimmer, G.J. Rees, R.C. Tozer, M. Hopkinson, and G. Hill, *Electron Devices, IEEE Trans.* **48**, 2198 (2001).
- <sup>12</sup> G.E. Bulman, V.M. Robbins, K.F. Brennan, K. Hess, and G.E. Stillman, *IEEE Electron Device Lett.* **4**, 181 (1983).
- <sup>13</sup> L.J.J. Tan, J.S. Ng, C.H. Tan, and J.P.R. David, *IEEE J. Quantum Electron.* **44**, 378 (2008).
- <sup>14</sup> O. Hildebrand, W. Kuebart, and M.H. Pilkuhn, *Appl. Phys. Lett.* **37**, 801 (1980).
- <sup>15</sup> M. Grzesik, J. Donnelly, E. Duerr, M. Manfra, M. Diagne, R. Bailey, G. Turner, and W. Goodhue,

Appl. Phys. Lett. **104**, 162103 (2014).

<sup>16</sup> K. Brennan and K. Hess, Phys. Rev. B **29**, (1984).

<sup>17</sup> M.A. Saleh, M.M. Hayat, P.P. Sotirelis, A.L. Holmes, J.C. Campbell, B.E.A. Saleh, and M.C. Teich, IEEE Trans. Electron Devices **48**, 2722 (2001).

<sup>18</sup> I. Vurgaftman, J.R. Meyer, and L.R. Ram-Mohan, J. Appl. Phys. **89**, 5815 (2001).

<sup>19</sup> S.R. Forrest, M. Didomenico, Jr., R.G. Smith, and S.H. J., Appl. Phys. Lett. **36**, 580 (1980).

<sup>20</sup> C. Benz, M. Claassen, and D. Liebig, J. Appl. Phys. **81**, 3181 (1997).